

里德-所罗门编码联合分集接收系统对海洋湍流抑制性能研究

杨祎¹, 邱晓芬^{1*}, 王晓波², 张建磊¹, 和晗昱¹, 聂欢¹, 刘浩宇¹

¹西安邮电大学电子工程学院, 陕西 西安 710121;

²中国船舶集团公司第 705 研究所水下信息与控制重点实验室, 陕西 西安 710077

摘要 针对水下无线激光通信链路性能劣化问题, 基于 Yue 谱推导了在包含有限外尺度和海洋水体分层不稳定性度的弱海洋湍流信道下高斯光束的空间相干半径和闪烁指数闭合解析式, 量化了基于高斯光束的海洋分集接收系统中的湍流强度和探测器间距阈值。在此基础上设计了一种基于高斯光束的里德-所罗门(RS)编码联合均衡等增益合并(EEGC)算法的单入多出(SIMO)通信系统。利用双曲正切函数法推导了系统的上限平均误码率(ABER)闭合解析式, 并研究了海洋水体分层的不稳定程度和探测器分布方式对系统性能的影响。仿真结果表明, 海洋水体分层的稳定与否对系统性能影响较为明显。此外, 所设计的系统可有效抑制复合海洋信道下高斯光束的湍流效应, 湍流越强, 抑制效果越显著; 也可有效降低探测器的分布方式对采用高斯光束传输的 SIMO 系统性能的影响。

关键词 无线光传输; 海洋湍流; 高斯光束; 分集接收; 里德-所罗门编码

中图分类号 TN929.12

文献标志码 A

DOI: 10.3788/AOS230454

1 引言

随着水下运载器和海洋传感网络的大规模部署, 水下高速无线光通信系统成为获取数据的重要平台。分析光束在海洋湍流中引起的闪烁和波束传输特性, 探索有效的海洋湍流抑制技术已成为构建高稳定性、高速率、远距离传输的水下无线激光通信系统的核心要点之一^[1-2]。

研究证明, 海洋湍流引起的光强闪烁以及波束传播特性会受海水折射率起伏变化的影响^[3-4]。Nikishov 等^[5]在将海洋水体分层视为稳定状态的情况下首次推导了海洋湍流折射率波动的精确功率谱。Ata 等^[6]和 Lu 等^[7]基于 Nikishov 谱^[5]分别推导了平面波和球面波在海洋湍流信道中的闪烁指数、波结构函数以及空间相干半径的闭合解析式。Gerçekcioğlu^[8]和 Wang 等^[9]推导了弱海洋湍流信道中高斯光束的闪烁指数解析式。针对实际海洋环境中盐分转移和热扩散机理不一致导致的水体分层不稳定问题, Elamassie 等^[10]建立了包含水体分层不稳定性度的海洋湍流折射率功率谱, 并分析了平面波和球面波在该模型下的闪烁特性。建立在无限外尺度基础上的折射率功率谱会导致极点处可能存在奇点问题, 且不符合真实的海洋传输环境, 因

此, 研究者们相继提出了包含水体分层不稳定性度和有限外尺度的修正海洋折射率功率谱——Yue 谱^[11]和 Li 谱^[12]。Luan 等^[13]基于 Yue 谱^[11]推导了平面波和球面波的闪烁指数闭合解析式。

近年来, 研究人员提出利用空间分集^[14-16]、信道编码^[17-18]等技术来抑制海洋湍流的影响。单入多出(SIMO)链路是应用于水下无线激光通信系统中最常见的一种分集接收技术, 它利用多个探测器生成并行分集路径, 可有效抑制海洋湍流引起的闪烁特性^[19]。Liu 等^[20]利用蒙特卡罗仿真方法证明了弱海洋湍流中 SIMO 系统采用等增益合并(EGC)算法性能最优。Boucoulalas 等^[21]将光放大技术与 EGC SIMO 系统结合, 进一步改善了系统性能。Jamali 等^[22]在水下光通信多人多出(UOWC MIMO)通信系统中利用 Gauss-Hermite 正交积分法推导得到了基于平面波的精确 EGC 和上限平均误码率(ABER)表达式。然而, 海洋中鱼群和大型水生动物频繁活动可能会在某个时间点内持续遮挡传输信号, 阻断传输路径, 导致传输数据流出现突发或随机错误。因此, Ramavath 等^[23]利用里德-所罗门(RS)编码技术提升了采用平面波传输的 UOWC MIMO 通信系统中数据的完整性。上述研究均在基于 Nikishov 谱的海洋信道中分析空间分集技术

收稿日期: 2023-01-09; 修回日期: 2023-02-14; 录用日期: 2023-03-12; 网络首发日期: 2023-05-08

基金项目: 装备预研教育部联合基金(8091B032130)、水下信息与控制重点实验室资助项目(JCKY2021207CD02)、陕西省微波光光子与光通信创新团队(2021TD-09)

通信作者: *shiguozhi907@163.com

传输特性,在包含有限外尺度以及水体分层不稳定的海洋湍流信道下基于高斯光束的 SIMO 系统特性分析未见报道。

为进一步抑制湍流对基于高斯光束的系统性能的影响,本文在考虑吸收、散射造成的路径损耗和包含水体分层不稳定性及有限外尺度的湍流复合信道后,研究了采用高斯光束传输的 RS 编码联合 SIMO 通信系统的传输性能。首先,推导在包含海洋水体分层不稳定性及有限外尺度的海洋湍流模型下高斯光束的闪烁指数和空间相干半径的闭合解析式,确定 SIMO 系统的探测器间距阈值以及湍流的强度。其次,提出一种校正因子来均衡海洋信道中高斯光束非线性的合并

算法,并将 RS 编码技术与均衡等增益合并(EEGC)算法结合来抑制海洋 SIMO 系统传输过程中的湍流效应,进一步推导系统的上限 ABER 闭合表达式。最后,分析海洋水体分层的不稳定程度、探测器分布方式和分集接收合并算法对弱海洋湍流信道下基于高斯光束的系统性能的影响。

2 光学海洋湍流理论

Yue 等^[11]考虑海洋有限外尺度和水体分层不稳定性等因素,基于 Elamassie 模型建立了更接近真实海洋传输环境的湍流折射率起伏空间功率谱模型。具体定义为

$$\Phi_n(\kappa) = (4\pi)^{-1} C_0 \varepsilon^{-1/3} A^2 \chi_T (\kappa^2 + \kappa_0^2)^{-11/6} \left\{ \left[1 + C_T (\kappa\eta)^{2/3} \right] \exp \left[-\frac{(\kappa\eta)^2}{N_T^2} \right] + \omega^{-2} d_r \left[1 + C_S (\kappa\eta)^{2/3} \right] \times \exp \left[-\frac{(\kappa\eta)^2}{N_S^2} \right] - \omega^{-1} (1 + d_r) \left[1 + C_{TS} (\kappa\eta)^{2/3} \right] \exp \left[-\frac{(\kappa\eta)^2}{N_{TS}^2} \right] \right\}, \quad (1)$$

式中:下标 n 表示折射率波动; κ 为海洋湍流功率谱空间波数^[10]; $C_0 = 0.72$; ε 为湍流动能耗散率, $\varepsilon \in [10^{-10}, 10^{-1}]$; A 为热膨胀系数; χ_T 为均方温差耗散率; $\kappa_0 = 2\pi/L_0$ 表示空间截止频率, L_0 为外尺度尺寸; $C_j, j = T, S, TS$ 分别表示温度、盐度、温盐耦合对应的结构常数; η 为 Kolmogorov 内尺度; ω 为湍流中温度和盐度的相对强度, $\omega \in [-5, 0]$ (当 $|\omega| < 1$ 时,盐度波动主导光学海洋湍流,当 $|\omega| > 1$ 时,温度波动主导光学海洋湍流^[24]); $N_j = 3Q^{-3/2} \left(W_j - \frac{1}{3} + \frac{1}{9W_j} \right)^{3/2}$, 其中, $Q = 2.35$, $W_j = \left\{ \left[1/27 - (P_{Tj} Q^2)/(6C_0) \right]^2 - 1/729 \right\}^{1/2} - \left[1/27 - (P_{Tj} Q^2)/(6C_0) \right]^{1/3}$, $j = T, S, TS$ ($P_{Tj}, j = T, S, TS$ 分别表示温度、盐度、温盐耦合的普朗特数); d_r 为海洋温盐涡流扩散比, $d_r = 1$ 即海洋水体分层呈稳定状态,当海洋水体分层不稳定性时, d_r 表示^[10]为

$$d_r \approx \begin{cases} |\omega| \left[|\omega| - \sqrt{|\omega|(|\omega| - 1)} \right], & |\omega| \geq 1 \\ (1.85 - 0.85|\omega|^{-1})|\omega|, & 0.5 \leq |\omega| \leq 1 \\ 0.15|\omega|, & |\omega| < 0.5 \end{cases} \quad (2)$$

在水下无线激光通信系统中,闪烁指数是衡量海洋湍流对激光传输特性影响的重要参数,用以描述经过湍流后接收端光强波动的大小^[25]。空间相干半径通常作为重要参数来衡量经过海洋湍流后光束光强起伏的强弱范围^[26]。湍流强度可通过闪烁指数进行具体量化。

2.1 高斯光束的闪烁指数

对于高斯光束,在各向均匀同性的弱海洋湍流下其闪烁指数定义^[27]为

$$\delta_{I,OT}^2(L_0, L) = 8\pi^2 k^2 L \int_0^\infty \int_0^\infty \kappa \Phi_n(\kappa) \exp \left(-\frac{\Lambda L \kappa^2 \xi^2}{k} \right) \left\{ I_0(2\Lambda \rho \xi \kappa) - \cos \left[L \kappa^2 \xi \left(1 - \bar{\Theta} \xi \right) / k \right] \right\} d\kappa d\xi, \quad (3)$$

式中: L 为光束在海洋中的传输距离; $k = 2\pi/\lambda$ 为波数, λ 为波长; ρ 为波阵面上光束两点间的距离; ξ 为距离变量; $\Lambda = \Lambda_0 / (\Theta_0^2 + \Lambda_0^2)$ 表示光束接收参数,其中, Θ_0 和 Λ_0 表示发射光束参数, $\Lambda_0 = 2L / (k\omega_0^2)$, ω_0 为发射平面束腰半径; $\bar{\Theta} = 1 - \Theta$, $\Theta = \Theta_0 / (\Theta_0^2 + \Lambda_0^2)$; $I_0(\cdot)$ 表示修正的零阶贝塞尔函数, $I_0(x) = 1 + \sum_{n=1}^\infty (x/2)^{2n} / [n! \Gamma(n+1)]$, $\Gamma(\cdot)$ 表示 Gamma 函数。

对于高斯光束而言,在弱海洋湍流信道下其闪烁指数可定义为径向分量和纵向分量之和^[27]。径向分量和纵向分量分别表示为

$$\delta_r^2(L_0, L) = 8\pi^2 k^2 L \int_0^\infty \int_0^\infty \kappa \Phi_n(\kappa) \exp \left(-\Lambda L \kappa^2 \xi^2 / k \right) \left[I_0(2\Lambda \rho \xi \kappa) - 1 \right] d\kappa d\xi, \quad (4)$$

$$\delta_{i,i}^2(L_0, L) = 8\pi^2 k^2 L \int_0^1 \int_0^\infty \kappa \Phi_n(\kappa) \exp\left(-\frac{\Delta L \kappa^2 \xi^2}{k}\right) \left\{1 - \cos\left[L \kappa^2 \xi \left(1 - \bar{\Theta} \xi\right) / k\right]\right\} d\kappa d\xi. \quad (5)$$

将 Yue 谱式(1)与式(4)结合, 高斯光束在包含有限外尺度和水体分层不稳定程度的弱海洋湍流中的径向闪烁指数表示为

$$\delta_{i,r}^2(L_0, L) = 2\pi k^2 L C_0 \varepsilon^{-1/3} A^2 \chi_T \int_0^1 \int_0^\infty \kappa (\kappa^2 + \kappa_0^2)^{-11/6} \sum_{n=1}^\infty \frac{(\Delta \rho \xi \kappa)^{2n}}{(n!)^2} \left\{ \left[1 + C_T (\kappa \eta)^{2/3}\right] \exp\left\{-\left[\frac{\Delta L \kappa^2 \xi^2}{k} + \frac{(\kappa \eta)^2}{N_T^2}\right]\right\} + \frac{d_r \left[1 + C_S (\kappa \eta)^{2/3}\right]}{\omega^2} \exp\left\{-\left[\frac{\Delta L \kappa^2 \xi^2}{k} + \frac{(\kappa \eta)^2}{N_S^2}\right]\right\} - \frac{(1 + d_r) \left[1 + C_{TS} (\kappa \eta)^{2/3}\right]}{\omega} \exp\left\{-\left[\frac{\Delta L \kappa^2 \xi^2}{k} + \frac{(\kappa \eta)^2}{N_{TS}^2}\right]\right\} \right\} d\kappa d\xi, \quad (6)$$

将文献[28]中第二类合流超几何函数的积分表达式与式(6)结合, 可得

$$\int_{n=0}^\infty \kappa^{2t} (\kappa^2 + \kappa_0^2)^{-11/6} \exp(-\kappa_0^2 / \kappa_1^2) d\kappa \approx \frac{1}{2} \kappa_0^{2(t-4/3)} \Gamma\left(t + \frac{1}{2}\right) \left[\frac{\Gamma(4/3 - t)}{\Gamma(11/6)} + \frac{\Gamma(t - 4/3)}{\Gamma(t + 1/2)} \left(\frac{\kappa_0^2}{\kappa_1^2}\right)^{4/3-t} \right], \quad \kappa_0^2 / \kappa_1^2 \ll 1, \quad (7)$$

式中, t 为被积变量。

利用式(7)可将式(6)重新表示为

$$\delta_{i,r}^2(L_0, \rho, L) = \pi k^2 L C_0 \varepsilon^{-1/3} A^2 \chi_T \int_0^1 \sum_{n=1}^\infty \frac{(\Delta \rho \xi)^{2n}}{n!} \kappa_0^{2(n-5/6)} \left\{ \frac{\Gamma(5/6 - n)}{\Gamma(11/6)} \left(1 + \frac{d_r}{\omega^2} - \frac{1 + d_r}{\omega}\right) + \frac{\Gamma(n - 5/6)}{\Gamma(n + 1)} \kappa_0^{5/3-2n} \times \left[\left(\frac{\Delta L \xi^2}{k} + \frac{\eta^2}{N_T^2}\right)^{5/6-n} + \frac{d_r}{\omega^2} \left(\frac{\Delta L \xi^2}{k} + \frac{\eta^2}{N_S^2}\right)^{5/6-n} - \frac{1 + d_r}{\omega} \left(\frac{\Delta L \xi^2}{k} + \frac{\eta^2}{N_{TS}^2}\right)^{5/6-n} \right] d\xi + \eta^{2/3} \int_0^1 \sum_{n=1}^\infty \frac{(\Delta \rho \xi)^{2n} \Gamma(n + 4/3)}{(n!)^2} \times \kappa_0^{2n-1} \left\{ \frac{\Gamma(1/2 - n)}{\Gamma(11/6)} \left(C_T + C_S \frac{d_r}{\omega^2} - C_{TS} \frac{1 + d_r}{\omega}\right) + \frac{\Gamma(n - 1/2)}{\Gamma(n + 4/3)} \kappa_0^{1-2n} \left[C_T \left(\frac{\Delta L \xi^2}{k} + \frac{\eta^2}{N_T^2}\right)^{1/2-n} + C_S \frac{d_r}{\omega^2} \left(\frac{\Delta L \xi^2}{k} + \frac{\eta^2}{N_S^2}\right)^{1/2-n} - C_{TS} \frac{(1 + d_r)}{\omega} \left(\frac{\Delta L \xi^2}{k} + \frac{\eta^2}{N_{TS}^2}\right)^{1/2-n} \right] d\xi \right\}, \quad (8)$$

将超几何函数 ${}_2F_1(a_i, b_i; c_i; x)$ 的积分性质^[28]与式(8)结合, 可得

$$\int_0^1 \xi^{2n} \left(\frac{\Delta L \xi^2}{k} + \frac{\eta^2}{N_j^2}\right)^{a_i-n} d\xi = \frac{1}{2} \frac{\Gamma(n + 1/2)}{\Gamma(n + 3/2)} \left(\frac{\eta}{N_j}\right)^{2a_i-2n} {}_2F_1\left(n - a_i, n + 1/2; n + 3/2; -\frac{N_j^2 \Delta L}{\eta^2 k}\right), \quad (9)$$

利用式(9)化简式(8)可得到高斯光束在弱海洋信道中的径向闪烁指数闭合解析式, 表示为

$$\sigma_{i,r}^2(L_0, L, \rho) = \pi k^2 L C_0 \varepsilon^{-1/3} A^2 \chi_T \left\{ \sum_{n=1}^\infty \frac{(\Delta \rho)^{2n}}{n!} \kappa_0^{2(n-5/6)} \left\{ \frac{\Gamma(5/6 - n)}{\Gamma(11/6) (2n + 1)} \left(1 + \frac{d_r}{\omega^2} - \frac{1 + d_r}{\omega}\right) + \frac{\Gamma(n - 5/6)}{\Gamma(n + 1)} \right\} \times \kappa_0^{5/3-2n} \left[M\left(N_T, n, \frac{5}{6}\right) + \frac{d_r}{\omega^2} M\left(N_S, n, \frac{5}{6}\right) - \frac{1 + d_r}{\omega} M\left(N_{TS}, n, \frac{5}{6}\right) \right] \right\} + \eta^{2/3} \sum_{n=1}^\infty \frac{(\Delta \rho)^{2n} \Gamma(n + 4/3)}{(n!)^2} \times \kappa_0^{2n-1} \left\{ \frac{\Gamma(1/2 - n)}{\Gamma(11/6) (2n + 1)} \left(C_T + C_S \frac{d_r}{\omega^2} - C_{TS} \frac{1 + d_r}{\omega}\right) + \frac{\Gamma(n - 1/2)}{\Gamma(n + 4/3)} \times \kappa_0^{1-2n} \left[C_T M\left(N_T, n, \frac{1}{2}\right) + C_S \frac{d_r}{\omega^2} M\left(N_S, n, \frac{1}{2}\right) - C_{TS} \frac{1 + d_r}{\omega} M\left(N_{TS}, n, \frac{1}{2}\right) \right] \right\}, \quad (10)$$

$$\text{式中, } M(N_j, n, \beta) = \frac{\Gamma(n + 1/2)}{2(n + 3/2)} \left(\frac{\eta}{N_j}\right)^{2\beta-2n} {}_2F_1\left(n - \beta, n + 1/2; n + 3/2; -\frac{N_j^2 \Delta L}{\eta^2 k}\right).$$

结合式(1)与式(5)可建立在考虑海洋水体分层不稳定以及有限外尺度的弱海洋湍流中高斯光束的纵向闪烁指数模型, 表示为

$$\begin{aligned}
 \sigma_{i,i}^2(L_0, L) = & 2\pi k^2 LC_0 \epsilon^{-1/3} A^2 \chi_T \int_0^{\infty} \kappa (\kappa^2 + \kappa_0^2)^{-11/6} \left\{ [1 + C_T (\kappa\eta)^{2/3}] \exp \left\{ - \left[\frac{\Delta L \kappa^2 \xi^2}{k} + \frac{(\kappa\eta)^2}{N_T^2} \right] \right\} + \frac{d_r}{\omega^2} [1 + C_S (\kappa\eta)^{2/3}] \times \right. \\
 & \left. \exp \left\{ - \left[\frac{\Delta L \kappa^2 \xi^2}{k} + \frac{(\kappa\eta)^2}{N_S^2} \right] \right\} - \frac{1 + d_r}{\omega} [1 + C_{TS} (\kappa\eta)^{2/3}] \exp \left\{ - \left[\frac{\Delta L \kappa^2 \xi^2}{k} + \frac{(\kappa\eta)^2}{N_{TS}^2} \right] \right\} \right\} d\kappa d\xi - \\
 & 2\pi k^2 LC_0 \epsilon^{-1/3} A^2 \chi_T \int_0^{\infty} \kappa (\kappa^2 + \kappa_0^2)^{-11/6} \operatorname{Re} \left\{ [1 + C_T (\kappa\eta)^{2/3}] \exp \left\{ - \left[\frac{L \kappa^2 \xi (1 - \bar{\Theta} \xi) i}{k} + \frac{\Delta L \kappa^2 \xi^2}{k} + \frac{(\kappa\eta)^2}{N_T^2} \right] \right\} + \right. \\
 & \left. \frac{d_r [1 + C_S (\kappa\eta)^{2/3}]}{\omega^2} \times \exp \left\{ - \left[\frac{L \kappa^2 \xi (1 - \bar{\Theta} \xi) i}{k} + \frac{\Delta L \kappa^2 \xi^2}{k} + \frac{(\kappa\eta)^2}{N_S^2} \right] \right\} - \frac{(1 + d_r)}{\omega} [1 + C_{TS} (\kappa\eta)^{2/3}] \times \right. \\
 & \left. \exp \left\{ - \left[\frac{L \kappa^2 \xi (1 - \bar{\Theta} \xi) i}{k} + \frac{\Delta L \kappa^2 \xi^2}{k} + \frac{(\kappa\eta)^2}{N_{TS}^2} \right] \right\} \right\} d\kappa d\xi, \tag{11}
 \end{aligned}$$

式中, $\operatorname{Re}(\cdot)$ 表示复数的实部。

利用式(7)可将式(11)化简为仅包含变量 ξ 的积分, 即

$$\begin{aligned}
 \sigma_{i,i}^2(L_0, L) = & \pi k^2 LC_0 \epsilon^{-1/3} A^2 \chi_T \left\{ \Gamma(-5/6) \left[\left(\frac{\Delta L \xi^2}{k} + \frac{\eta^2}{N_T^2} \right)^{5/6} + \frac{d_r}{\omega^2} \left(\frac{\Delta L \xi^2}{k} + \frac{\eta^2}{N_S^2} \right)^{5/6} - \frac{1 + d_r}{\omega} \left(\frac{\Delta L \xi^2}{k} + \frac{\eta^2}{N_{TS}^2} \right)^{5/6} \right] + \right. \\
 & \left. \eta^{2/3} \Gamma(-1/2) \left[C_T \left(\frac{\Delta L \xi^2}{k} + \frac{\eta^2}{N_T^2} \right)^{1/2} + \frac{d_r}{\omega^2} C_S \left(\frac{\Delta L \xi^2}{k} + \frac{\eta^2}{N_S^2} \right)^{1/2} - \frac{1 + d_r}{\omega} C_{TS} \left(\frac{\Delta L \xi^2}{k} + \frac{\eta^2}{N_{TS}^2} \right)^{1/2} \right] \right\} d\xi - \\
 & \pi k^2 LC_0 \epsilon^{-1/3} A^2 \chi_T \times \operatorname{Re} \left\{ \Gamma(-5/6) \left[\left[\frac{\Delta L \xi^2}{k} + \frac{\eta^2}{N_T^2} + \frac{L \xi (1 - \bar{\Theta} \xi) i}{k} \right]^{5/6} + \frac{d_r}{\omega^2} \left[\frac{\Delta L \xi^2}{k} + \frac{\eta^2}{N_S^2} + \frac{L \xi (1 - \bar{\Theta} \xi) i}{k} \right]^{5/6} - \right. \right. \\
 & \left. \frac{1 + d_r}{\omega} \left[\frac{\Delta L \xi^2}{k} + \frac{\eta^2}{N_{TS}^2} + \frac{L \xi (1 - \bar{\Theta} \xi) i}{k} \right]^{5/6} \right\} + \eta^{2/3} \Gamma(-1/2) \left\{ C_T \left[\frac{\Delta L \xi^2}{k} + \frac{\eta^2}{N_T^2} + \frac{L \xi (1 - \bar{\Theta} \xi) i}{k} \right]^{1/2} + \right. \\
 & \left. C_S \frac{d_r}{\omega^2} \left[\frac{\Delta L \xi^2}{k} + \frac{\eta^2}{N_S^2} + \frac{L \xi (1 - \bar{\Theta} \xi) i}{k} \right]^{1/2} - \frac{1 + d_r}{\omega} C_{TS} \left[\frac{\Delta L \xi^2}{k} + \frac{\eta^2}{N_{TS}^2} + \frac{L \xi (1 - \bar{\Theta} \xi) i}{k} \right]^{1/2} \right\} d\xi. \tag{12}
 \end{aligned}$$

依据 ${}_2F_1(-\vartheta, \vartheta + 1; \vartheta + 2; x) = \left(1 - \frac{2}{3}x\right)^{\vartheta}$ [29] 和 ${}_2F_1(1 - \beta, 1; 2; x) = \frac{(1-x)^{\beta} - 1}{\beta x}$ [28], 结合式(12)可得

$$\begin{aligned}
 \int_0^1 \left[\frac{\Delta L \xi^2}{k} + \frac{\eta^2}{N_j^2} + \frac{L \xi (1 - \bar{\Theta} \xi) i}{k} \right]^{\vartheta} d\xi = & \left(\frac{\eta}{N_j} \right)^{2\vartheta} \frac{1}{3^{\vartheta}} \left(\frac{LN_j^2}{k\eta^2} \right)^{\vartheta+1} \frac{\left\{ \sqrt{[3k\eta^2 / (LN_j^2) + 2\Delta]^2 + (3 - 2\bar{\Theta})^2} \right\}^{\vartheta+1} \cos[(\vartheta + 1)\varphi_1 - \varphi_2] - \cos \varphi_2}{\left(\frac{LN_j^2}{k\eta^2} \right) (\vartheta + 1) \sqrt{4\Delta^2 + (3 - 2\bar{\Theta})^2}}, \tag{13}
 \end{aligned}$$

式中: $\varphi_1 = \arctan \left[\frac{3 - 2\bar{\Theta}}{3k\eta^2 / (LN_j^2) + 2\Delta} \right]$; $\varphi_2 = \arctan \left(\frac{3 - 2\bar{\Theta}}{2\Delta} \right)$ 。

利用式(13)可对式(12)进行去积分处理, 进而得到高斯光束纵向闪烁指数表达式, 即

$$\begin{aligned} \sigma_{i,i}^2(L_0, L) = & \pi k^2 L C_0 \epsilon^{-1/3} A^2 \chi_T \left\{ \Gamma(-5/6) \left[P\left(N_T, \frac{5}{6}\right) + \frac{d_r}{\omega^2} P\left(N_S, \frac{5}{6}\right) - \frac{1+d_r}{\omega} P\left(N_{TS}, \frac{5}{6}\right) - Q\left(N_T, \frac{5}{6}\right) - \right. \right. \\ & \left. \frac{d_r}{\omega^2} Q\left(N_S, \frac{5}{6}\right) + \frac{1+d_r}{\omega} Q\left(N_{TS}, \frac{5}{6}\right) \right] + \eta^{2/3} \Gamma(-1/2) \times \left[C_T P\left(N_T, \frac{1}{2}\right) + \frac{d_r}{\omega^2} C_S P\left(N_S, \frac{1}{2}\right) - \frac{1+d_r}{\omega} C_{TS} P\left(N_{TS}, \frac{1}{2}\right) - \right. \\ & \left. \left. C_T Q\left(N_T, \frac{1}{2}\right) - \frac{C_S d_r}{\omega^2} Q\left(N_S, \frac{1}{2}\right) + \frac{1+d_r}{\omega} C_{TS} Q\left(N_{TS}, \frac{1}{2}\right) \right] \right\}, \end{aligned} \quad (14)$$

式中：
$$P(N_j, \beta) = (\eta/N_j)^{2\beta} {}_2F_1\left[-\beta, 1/2; 3/2; -N_j^2 \Delta L / (\eta^2 k)\right]; \quad Q(N_j, \vartheta) = \left(\frac{\eta}{N_j}\right)^{2\vartheta} \frac{\frac{1}{3^\vartheta} \left(\frac{LN_j^2}{k\eta^2}\right)^{\vartheta+1} \left\{ \sqrt{[3k\eta^2 / (LN_j^2) + 2\Delta]^2 + (3 - 2\bar{\Theta})^2} \right\}^{\vartheta+1} \cos[(\vartheta + 1)\varphi_1 - \varphi_2] - \cos \varphi_2}{\left(\frac{LN_j^2}{k\eta^2}\right) (\vartheta + 1) \sqrt{4\Delta^2 + (3 - 2\bar{\Theta})^2}}.$$

针对外尺度有限且水体分层不稳定的弱海洋湍流信道, 利用式(10)和式(14)可推导得到高斯光束在惯性范围内($\rho \gg \eta$)的闪烁指数闭合解析式, 即

$$\begin{aligned} \delta_{i,OT}^2(L_0, L, \rho) = & \pi k^2 L C_0 \epsilon^{-1/3} A^2 \chi_T \left\{ \sum_{n=1}^{\infty} \frac{(\Delta\rho)^{2n}}{n!} \kappa_0^{2(n-5/6)} \left\{ \frac{\Gamma(5/6-n)}{\Gamma(11/6)(2n+1)} \left(1 + \frac{d_r}{\omega^2} - \frac{1+d_r}{\omega}\right) + \right. \right. \\ & \left. \frac{\Gamma(n-5/6)}{\Gamma(n+1)} \kappa_0^{5/3-2n} \left[M\left(N_T, n, \frac{5}{6}\right) + \frac{d_r}{\omega^2} M\left(N_S, n, \frac{5}{6}\right) - \frac{1+d_r}{\omega} M\left(N_{TS}, n, \frac{5}{6}\right) \right] \right\} + \\ & \eta^{2/3} \sum_{n=1}^{\infty} \frac{(\Delta\rho)^{2n} \Gamma(n+4/3)}{(n!)^2} \kappa_0^{2n-1} \left\{ \frac{\Gamma(1/2-n)}{\Gamma(11/6)(2n+1)} \left(C_T + C_S \frac{d_r}{\omega^2} - C_{TS} \frac{1+d_r}{\omega} \right) + \right. \\ & \left. \frac{\Gamma(n-1/2)}{\Gamma(n+4/3)} \kappa_0^{1-2n} \left[C_T M\left(N_T, n, \frac{1}{2}\right) + C_S \frac{d_r}{\omega^2} M\left(N_S, n, \frac{1}{2}\right) - C_{TS} \frac{1+d_r}{\omega} M\left(N_{TS}, n, \frac{1}{2}\right) \right] \right\} \left. \right\} + \pi k^2 L C_0 \epsilon^{-1/3} A^2 \chi_T \times \\ & \left\{ \Gamma(-5/6) \left[P\left(N_T, \frac{5}{6}\right) + \frac{d_r}{\omega^2} P\left(N_S, \frac{5}{6}\right) - \frac{1+d_r}{\omega} P\left(N_{TS}, \frac{5}{6}\right) - Q\left(N_T, \frac{5}{6}\right) - \frac{d_r}{\omega^2} Q\left(N_S, \frac{5}{6}\right) + \frac{1+d_r}{\omega} Q\left(N_{TS}, \frac{5}{6}\right) \right] + \right. \\ & \left. \eta^{2/3} \Gamma(-1/2) \times \right. \\ & \left. \left[C_T P\left(N_T, \frac{1}{2}\right) + \frac{d_r}{\omega^2} C_S P\left(N_S, \frac{1}{2}\right) - \frac{1+d_r}{\omega} C_{TS} P\left(N_{TS}, \frac{1}{2}\right) - C_T Q\left(N_T, \frac{1}{2}\right) - \frac{C_S d_r}{\omega^2} Q\left(N_S, \frac{1}{2}\right) + C_{TS} \frac{1+d_r}{\omega} Q\left(N_{TS}, \frac{1}{2}\right) \right] \right\}. \end{aligned} \quad (15)$$

2.2 高斯光束的空间相干半径

利用 Rytov 近似方法^[27]可将高斯光束的波结构函数表示为

$$\begin{aligned} D(\rho, L, L_0) = & 8\pi^2 k^2 L \int_0^1 \int_0^\infty \kappa \Phi_n(\kappa) \exp(-\Delta L \kappa^2 \xi^2 / k) \left\{ I_0(\Delta \rho \xi \kappa) - J_0[(1 - \bar{\Theta} \xi) \kappa \rho] \right\} d\kappa d\xi = \\ & \sigma_{i,r}\left(L, L_0, \frac{\rho}{2}\right) + D_o(L, L_0, \rho), \end{aligned} \quad (16)$$

式中, $J_0(\cdot)$ 表示零阶贝塞尔函数, $J_0(x) = 1 + \sum_{n=1}^{\infty} \left\{ (-1)^n (x/2)^{2n} / [n! \Gamma(n+1)] \right\}$ 。

根据 Yue 谱式(1)和式(16), $D_o(L, L_0, \rho)$ 的解析式可表示为

$$\begin{aligned} D_o(L, L_0, \rho) = & 2\pi k^2 L C_0 \epsilon^{-1/3} A^2 \chi_T \int_0^1 \int_0^\infty \frac{\kappa}{(\kappa^2 + \kappa_0^2)} \exp\left(-\frac{\Delta L \kappa^2 \xi^2}{k}\right) \frac{[(1 - \bar{\Theta} \xi) \kappa \rho]^2}{4} \times \\ & \left\{ \left[1 + C_T (\kappa \eta)^{2/3} \right] \exp\left[-\frac{(\kappa \eta)^2}{N_T^2}\right] + \frac{d_r [1 + C_S (\kappa \eta)^{2/3}]}{\omega^2} \exp\left[-\frac{(\kappa \eta)^2}{N_S^2}\right] - \frac{1+d_r}{\omega} [1 + C_{TS} (\kappa \eta)^{2/3}] \exp\left[-\frac{(\kappa \eta)^2}{N_{TS}^2}\right] \right\} d\kappa d\xi, \end{aligned} \quad (17)$$

式中, $J_0(x) \approx 1 - x^2/4, x > 0$ 。

利用式(7)和广义超几何函数的积分性质^[27]式(18)对式(17)去积分得到 $D_o(L, L_0, \rho)$ 的闭合解析式, 表示为

$$\int_0^x t^{\mu-1}(1+\beta t)^{\nu} dt = \frac{x^{\mu}}{\mu} {}_2F_1(\nu, \mu; \mu+1; -\beta x), \mu > 0, \quad (18)$$

$$\begin{aligned} D_o(L, L_0, \rho) = & \frac{1}{4} \pi k^2 LC_0 \epsilon^{-1/3} A^2 \chi_T \rho^2 \kappa_0^{1/3} \left\{ \frac{\Gamma(-1/6)}{\Gamma(11/6)} \left(1 - \bar{\Theta} + \frac{\bar{\Theta}^2}{3} \right) \left(1 + \frac{d_r}{\omega^2} - \frac{1+d_r}{\omega} \right) + \right. \\ & \left. \Gamma(1/6) \kappa_0^{-1/3} \left[G(N_T, 1/6) + \frac{d_r}{\omega^2} G(N_S, 1/6) - \frac{1+d_r}{\omega} G(N_{TS}, 1/6) \right] \right\} + \\ & \frac{1}{4} \pi k^2 LC_0 \epsilon^{-1/3} A^2 \chi_T \eta^{2/3} \rho^2 \Gamma(7/3) \kappa_0 \left\{ \frac{\Gamma(-1/2)}{\Gamma(11/6)} \left(1 - \bar{\Theta} + \frac{\bar{\Theta}^2}{3} \right) \left(C_T + C_S \frac{d_r}{\omega^2} - C_{TS} \frac{1+d_r}{\omega} \right) + \right. \\ & \left. \frac{\Gamma(1/2)}{\Gamma(7/3)} \kappa_0^{-1} \left[C_T G\left(N_T, \frac{1}{2}\right) + C_S \frac{d_r}{\omega^2} G\left(N_S, \frac{1}{2}\right) - C_{TS} \frac{1+d_r}{\omega} G\left(N_{TS}, \frac{1}{2}\right) \right] \right\}, \quad (19) \end{aligned}$$

式中, $G(N_j, r) = \left(\frac{\eta}{N_j} \right)^{-2r} \left[{}_2F_1\left(r, 1/2; 3/2; -\frac{N_j^2 \Delta L}{\eta^2 k}\right) + \frac{\bar{\Theta}^2}{3} {}_2F_1\left(r, 3/2; 5/2; -\frac{N_j^2 \Delta L}{\eta^2 k}\right) - \bar{\Theta} {}_2F_1\left(r, 1; 2; -\frac{N_j^2 \Delta L}{\eta^2 k}\right) \right]$.

当 $\rho < \omega_0$ 时, 结合式(10), $\sigma_{i,r}^2(L, L_0, \rho/2)$ 的闭合解析式可近似表示为

$$\begin{aligned} \sigma_{i,r}^2\left(L, L_0, \frac{\rho}{2}\right) = & \pi k^2 LC_0 \epsilon^{-1/3} A^2 \chi_T \frac{(\Delta p)^2}{4} \left\{ \kappa_0^{1/3} \left[\frac{\Gamma(-1/6)}{3\Gamma(11/6)} \left(1 + \frac{d_r}{\omega^2} - \frac{1+d_r}{\omega} \right) + \right. \right. \\ & \left. \Gamma(1/6) \kappa_0^{-1/3} \left[M\left(N_T, 1, \frac{5}{6}\right) + \frac{d_r}{\omega^2} M\left(N_S, 1, \frac{5}{6}\right) - \frac{1+d_r}{\omega} M\left(N_{TS}, 1, \frac{5}{6}\right) \right] \right\} + \\ & \eta^{2/3} \Gamma(7/3) \kappa_0 \left\{ \frac{\Gamma(-1/2)}{3\Gamma(11/6)} \left(C_T + C_S \frac{d_r}{\omega^2} - C_{TS} \frac{1+d_r}{\omega} \right) + \right. \\ & \left. \frac{\Gamma(1/2)}{\Gamma(7/3)} \kappa_0^{-1} \left[C_T M\left(N_T, 1, \frac{1}{2}\right) + C_S \frac{d_r}{\omega^2} M\left(N_S, 1, \frac{1}{2}\right) - C_{TS} \frac{1+d_r}{\omega} M\left(N_{TS}, 1, \frac{1}{2}\right) \right] \right\}. \quad (20) \end{aligned}$$

针对外尺度有限且水体分层不稳定的弱海洋湍流信道, 结合式(19)和式(20)可推导得到在惯性范围内, 考虑有限外尺度及可变温盐涡流扩散比的弱海洋湍流, 高斯光束的波结构函数的闭合表达式, 即

$$\begin{aligned} D(\rho, L, L_0) = & \frac{1}{4} \pi k^2 LC_0 \epsilon^{-1/3} A^2 \chi_T \left\{ \rho^2 \kappa_0^{1/3} \left[\frac{\Gamma(-1/6)}{\Gamma(11/6)} \left(1 - \bar{\Theta} + \frac{\bar{\Theta}^2}{3} \right) \left(1 + \frac{d_r}{\omega^2} - \frac{1+d_r}{\omega} \right) + \right. \right. \\ & \left. \Gamma(1/6) \kappa_0^{-1/3} \left[G(N_T, 1/6) + \frac{d_r}{\omega^2} G(N_S, 1/6) - \frac{1+d_r}{\omega} G(N_{TS}, 1/6) \right] \right\} + \\ & \eta^{2/3} \rho^2 \Gamma(7/3) \kappa_0 \left\{ \frac{\Gamma(-1/2)}{\Gamma(11/6)} \left(1 - \bar{\Theta} + \frac{\bar{\Theta}^2}{3} \right) \left(C_T + C_S \frac{d_r}{\omega^2} - C_{TS} \frac{1+d_r}{\omega} \right) + \right. \\ & \left. \frac{\Gamma(1/2)}{\Gamma(7/3)} \kappa_0^{-1} \left[C_T G\left(N_T, \frac{1}{2}\right) + C_S \frac{d_r}{\omega^2} G\left(N_S, \frac{1}{2}\right) - C_{TS} \frac{1+d_r}{\omega} G\left(N_{TS}, \frac{1}{2}\right) \right] \right\} + \\ & \pi k^2 LC_0 \epsilon^{-1/3} A^2 \chi_T \frac{(\Delta p)^2}{4} \left\{ \kappa_0^{1/3} \left[\frac{\Gamma(-1/6)}{3\Gamma(11/6)} \left(1 + \frac{d_r}{\omega^2} - \frac{1+d_r}{\omega} \right) + \right. \right. \\ & \left. \Gamma(1/6) \kappa_0^{-1/3} \left[M\left(N_T, 1, \frac{5}{6}\right) + \frac{d_r}{\omega^2} M\left(N_S, 1, \frac{5}{6}\right) - \frac{1+d_r}{\omega} M\left(N_{TS}, 1, \frac{5}{6}\right) \right] \right\} + \\ & \eta^{2/3} \Gamma(7/3) \kappa_0 \left\{ \frac{\Gamma(-1/2)}{3\Gamma(11/6)} \left(C_T + C_S \frac{d_r}{\omega^2} - C_{TS} \frac{1+d_r}{\omega} \right) + \right. \\ & \left. \frac{\Gamma(1/2)}{\Gamma(7/3)} \kappa_0^{-1} \left[C_T M\left(N_T, 1, \frac{1}{2}\right) + C_S \frac{d_r}{\omega^2} M\left(N_S, 1, \frac{1}{2}\right) - C_{TS} \frac{1+d_r}{\omega} M\left(N_{TS}, 1, \frac{1}{2}\right) \right] \right\}. \quad (21) \end{aligned}$$

根据空间相干半径 ρ_0 的定义式 $D_{oc}(L_0, L, \rho/2) = 2^{[27]}$, 结合式 (21), 可推导得到在考虑水体分层不稳定和有限外尺度的弱海洋湍流信道下高斯光束的空间相干半径闭合解析式:

$$\begin{aligned} \rho_0^{-2} = & \frac{1}{4} \pi k^2 L C_0 \epsilon^{-1/3} A^2 \chi_T \left\{ \kappa_0^{1/3} \left[\frac{\Gamma(-1/6)}{\Gamma(11/6)} \left(1 - \bar{\Theta} + \frac{\bar{\Theta}^2}{3} \right) \left(1 + \frac{d_r}{\omega^2} - \frac{1+d_r}{\omega} \right) + \right. \right. \\ & \left. \Gamma(1/6) \kappa_0^{-1/3} \left[G(N_T, 1/6) + \frac{d_r}{\omega^2} G(N_S, 1/6) - \frac{1+d_r}{\omega} G(N_{TS}, 1/6) \right] \right\} + \\ & \eta^{2/3} \Gamma(7/3) \kappa_0 \left\{ \frac{\Gamma(-1/2)}{\Gamma(11/6)} \left(1 - \bar{\Theta} + \frac{\bar{\Theta}^2}{3} \right) \left(C_T + C_S \frac{d_r}{\omega^2} - C_{TS} \frac{1+d_r}{\omega} \right) + \right. \\ & \left. \frac{\Gamma(1/2)}{\Gamma(7/3)} \kappa_0^{-1} \left[C_T G\left(N_T, \frac{1}{2}\right) + C_S \frac{d_r}{\omega^2} G\left(N_S, \frac{1}{2}\right) - C_{TS} \frac{1+d_r}{\omega} G\left(N_{TS}, \frac{1}{2}\right) \right] \right\} + \\ & \pi k^2 L C_0 \epsilon^{-1/3} A^2 \chi_T \frac{A^2}{4} \left\{ \kappa_0^{1/3} \left[\frac{\Gamma(-1/6)}{3\Gamma(11/6)} \left(1 + \frac{d_r}{\omega^2} - \frac{1+d_r}{\omega} \right) + \right. \right. \\ & \left. \frac{\Gamma(1/6)}{\Gamma(2)} \kappa_0^{-1/3} \left[M\left(N_T, 1, \frac{5}{6}\right) + \frac{d_r}{\omega^2} M\left(N_S, 1, \frac{5}{6}\right) - \frac{1+d_r}{\omega} M\left(N_{TS}, 1, \frac{5}{6}\right) \right] \right\} + \\ & \eta^{2/3} \Gamma(7/3) \kappa_0 \left\{ \frac{\Gamma(-1/2)}{3\Gamma(11/6)} \left(C_T + C_S \frac{d_r}{\omega^2} - C_{TS} \frac{1+d_r}{\omega} \right) + \frac{\Gamma(1/2)}{\Gamma(7/3)} \kappa_0^{-1} \times \right. \\ & \left. \left[C_T M\left(N_T, 1, \frac{1}{2}\right) + C_S \frac{d_r}{\omega^2} M\left(N_S, 1, \frac{1}{2}\right) - C_{TS} \frac{1+d_r}{\omega} M\left(N_{TS}, 1, \frac{1}{2}\right) \right] \right\}. \end{aligned} \quad (22)$$

3 基于高斯光束的 RS 编码联合分集接收系统

基于高斯光束的 RS 编码联合 EEGC 算法的分集接收系统如图 1 所示。系统发射端使用 OOK(on-off keying) 调制和 RS 编码的复合结构。在发射端, 根据 RS 编码格式对信源信号进行编码, 并将生成的二进制码元序列加载到电光调制模块; 通过 OOK 调制电路和

高斯光源生成载有信息的信号脉冲激光, 发出的光信号在空间域的光强分布具有高斯函数特性。在接收端, 利用 M 个雪崩光电二极管 (APD) 构成的分集接收模块对经海水复合信道传输后的各接收支路的光信号进行光电转换; 将完成光电转换的电信号分别通过解调、BM-Chien 译码器译码恢复出各支路数据信号, 最后利用 EEGC 算法将各支路数据信号合并, 得到总的接收信号。

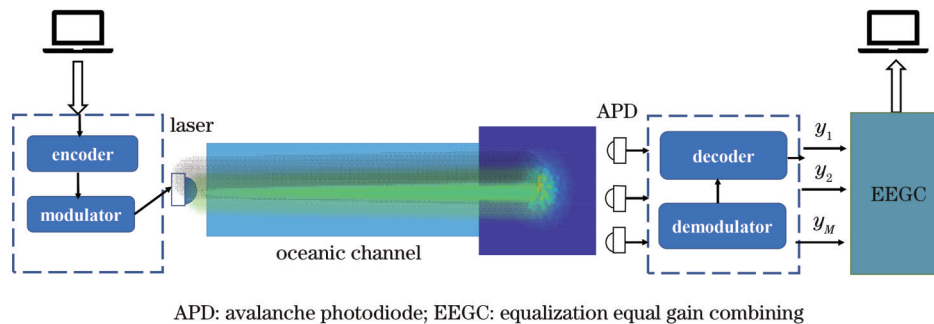


图 1 基于高斯光束的 RS 编码联合分集接收系统结构

Fig. 1 Structure of diversity receiver system with RS codes based on Gaussian beams

3.1 基于高斯光束的 EEGC 算法

假定高斯光束在弱海洋湍流信道传输一定距离后, 其接收端的光强分布仍近似为高斯分布。针对接收端光强不均匀导致的传统 SIMO 系统线性阵列中 EEGC 算法性能不佳的问题, 根据接收光强分布特性提出校正因子, 以距离光斑中心最近探测器的接收光强

为基准对各支路接收光强进行校准, 使得各支路接收光强均衡, 得到 EEGC 算法。当 APD 阵列分布根据接收光强分布特性分别采用对称分布和非对称分布时, 基于高斯光束的海洋 EEGC SIMO 系统结构如图 2(a)、(b) 所示。其中: $y_i, i = 1, 2, \dots, M$ 表示各支路的接收信号; Δl 表示探测器间的距离 (探测器间间距

的阈值下限由空间相干半径确定,当 $\Delta l > \rho_0$ 时,可保

证各支路接收信号的独立性)。

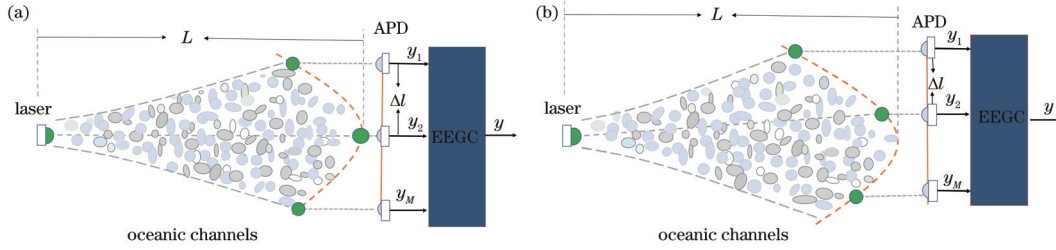


图 2 基于高斯光束的 EEGC SIMO 通信系统结构。(a) APD 对称分布; (b) APD 非对称分布

Fig. 2 Structure of EEGC SIMO system based on Gaussian beams. (a) APD symmetric distribution; (b) APD asymmetric distribution

高斯光束在海洋信道传输一定距离后,其接收平面内的光强分布表示为

$$I(r, L) = I'_0 \exp(-2r^2/\omega_L^2), \quad (23)$$

式中: r 为距离光束中心的径向距离; I'_0 为接收平面内的中心光强; ω_L 是传输距离为 L 时的束腰半径, 表示为 $\omega_L = \omega_0 \sqrt{1 + [\lambda L / (\pi \omega_0^2)]^2}$, 其中 ω_0 为束腰半径。

在基于高斯光束 EEGC 的 SIMO 系统中, 根据式 (23), 第 i 条支路的校正因子 τ_i 可通过距离光斑中心最近探测器的接收光强和当前支路接收光强之间的比值确定。当 APD 采用对称分布和非对称分布时, τ_i 分别定义为

$$\begin{cases} \tau_i = \exp(-2D_i^2/\omega_L^2) / \exp\{-2[D_i + (i - n_s)\Delta l]^2/\omega_L^2\}, & \text{for symmetric distribution} \\ \tau_i = \exp(-2D_i^2/\omega_L^2) / \exp\{-2[D_i + (i - 1)\Delta l]^2/\omega_L^2\}, & \text{for asymmetrical distribution} \end{cases}, \quad (24)$$

式中: $I_i = \max\{I_i\}$, I_i 表示经湍流信道后第 i 条支路的接收光强; D_i 为光斑中心到光强为 I_i 对应点的径向距离; i 为偶数时, $n_s = i/2$, i 为奇数时, $n_s = (i + 1)/2$ 。

在 OOK 调制的 SIMO 通信系统中, EEGC 算法合并后的总接收信号表示为

$$y = \sqrt{2(P_t \hbar G)^2 \frac{\sum_{i=1}^M I_i \tau_i s}{M}} + n_1, \quad (25)$$

式中: P_t 为发射功率; $s \in (0, 1)$ 为传输数据; G 为 APD 的增益; \hbar 为 APD 的响应度 (单位为 A/W); 在海洋湍流中 APD 的主要噪声为热噪声^[30], n_1 表示均值为零、方差为 σ^2 的独立信道加性高斯白噪声, $\sigma^2 = 4K_b T B / R_L$, 其中, K_b 和 T 分别表示带宽和开尔文温度, B 和 R_L 分别表示玻尔兹曼常数和等效负载电阻。

3.2 RS 码的编译码

定义在伽罗华域 $G_F(q)$ ($q = p^m$) 的 (n, k_H, t) RS 码, 其码长和纠错能力上限可分别表示为 $n = q - 1$ 和 $t = 0.5(n - k_H)$, k_H 为信息位。若 a 表示 $G_F(q)$ 的本原元且生成的多项式以 a^v ($v = 1, 2, \dots, 2t - 1$) 为根, 可将 (n, k_H, t) RS 码的生成多项式表示为 $g(x) = \prod_{v=1}^{2t-1} (x - a^v)$ 。在系统发射端的编码模块, 发射端生成的信息数据以每组 $k_H \cdot m$ 的形式进行分组, 从而确定信息多项式和校验多项式, 并结合生成多项式完成编码得到待调制的数据信息。发送码字多项式表示为 $C(x) = M(x) \times g(x)$, 其中, $M(x) = s_0 +$

$s_1 x + s_2 x^2 + \dots + s_{k_H-1} x^{k_H-1}$ 表示信息多项式。经过海洋信道传输后的接收信息数据通常包含信道诱导的噪声信息, 其接收码字多项式可表示为 $R(x) = r_{(0)} x + r_{(1)} x + r_{(2)} x + \dots + r_{(n-1)} x$, $R(x) \equiv C(x) + E(x)$, 其中 $E(x) = \sum_{\xi=1}^t y_\xi x^\xi$ 表示错误图样多项式,

$y_\xi \in G_F(q)$ 表示第 v 个发生错误位置的错误值。接收端通过 BM-Chien 译码器完成对接收数据信息进行 RS 编码的译码。在系统接收端的译码模块, 首先通过接收码字多项式确定伴随多项式, 表示为 $S(x) \equiv C(x) + E(x) \equiv R(x) \equiv E(x) \pmod{g(x)}$ 。其次利用 BM 迭代算法和 Chien 搜索法确定错误位置多项式 $\sigma(x) = \sum_{v=1}^t \sigma_v x^v$ 的根和系数, 进而确定接收码元的错误位置。所采用的 BM 迭代算法通过选择迭代初值 $\sigma^{(0)}(x)$, 根据迭代公式进行迭代计算直至迭代到 $\sigma^{(t)}(x)$, 得到错误图样多项式 $\sigma(x)$ 的系数; Chien 搜索算法接收信息从高位至低位开始逐位校验 (校验 $\sum_{\xi=1}^t \sigma_\xi [(\alpha^{-v})^{-\xi}]$ 的根), 若计算结果为 -1 , 即当前位置出现译码错误。最后依据错误位置和错误值可获得估计错误图样 $\hat{E}(x)$, 并得到译码后的信息 $\hat{C}(x) = R(x) - \hat{E}(x)$ 。

4 系统性能

在基于高斯光束的 (n, k_H, t) RS 编码联合弱海洋

湍流 EEGC SIMO 通信链路中, 信号数据源以每字节 $m = \log_2(n + 1)$ 位在伽罗华域 $G_F(2^m)$ 进行 RS 编码, 设最大纠错码元个数为 t 。假定经编码后的 OOK 信号传输只受 APD 热噪声和海洋信道的影响, 则系统上限 BER (bit error rate) 表示^[31]为

$$P_d = \sum_{v=1}^n \binom{n}{v} P_s (1 - P_s)^m, \quad (26)$$

式中, $P_s = 1 - (1 - P_{\text{SIMO}})^m$, 代表第 m 位 bit 的错误率, 其中, P_{SIMO} 表示未进行 RS 编码的弱海洋 EEGC SIMO 通信系统的 ABER (average BER), 表示为

$$P_{\text{SIMO}} = \int_0^\infty Q \left[\sqrt{\frac{2(P_i \hbar I_a G)^2}{\sigma^2}} \frac{1}{M} \sum_{i=1}^M I_i \tau_i \right] f(I_m) dI_m, \quad (27)$$

式中, $I_m = \sum_{i=1}^M I_i \tau_i$ 。

在考虑吸收、散射及包含水体分层不稳定性 and 有限外尺度的复合弱海洋湍流信道中, 系统总接收光强起伏的概率密度函数 (PDF)^[32] 表示为

$$f(I_m) = \frac{1}{2I_m \sqrt{2\pi\sigma_m^2}} \exp \left\{ -\frac{\left\{ \ln \left[I_m / (I_a I_g) \right] - 2u_m \right\}^2}{8\sigma_m^2} \right\}, \quad (28)$$

式中: I_a 为吸收衰减引起的波束损耗, $I_a = \exp[-c(\lambda)L]$ ^[33], 其中 $c(\lambda)$ 为吸收和散射引起的衰减系数; I_g 为几何损耗, $I_g = \pi \left(\frac{d_A}{2} \right)^2 / [\pi(\theta_i L)^2]$, 其中, d_A 为 APD 的接收孔径, θ_i 为光束发散角; u_m 和 σ_m^2 分别表示 EEGC 算法的均值和方差, $u_m = \frac{\ln(M)}{2} - \frac{\ln\{1 + [\exp(4\sigma_X^2) - 1]/M\}}{4}$, $\sigma_m^2 = \frac{\ln\{1 + [\exp(4\sigma_X^2) - 1]/M\}}{4}$, 其中 $\sigma_X^2 = [\ln(\sigma_{\text{I,OT}}^2 + 1)]/4$ 表示未分集信号的对应变量 $X = \ln(I_i/2)$ 服从弱海洋湍流信道后对应的方差。

利用双曲正切函数分布近似^[23]可将弱海洋湍流信道 PDF 式近似为

$$f_{I_m}(I_m) = \frac{b' \exp(2a) \left[I_m / (I_a I_g) \right]^{b'-1}}{\left\{ 1 + \exp(2a') \left[I_m / (I_a I_g) \right]^{b'} \right\}^2}, \quad (29)$$

式中: a', b' 为非线性拟合系数; a, b 为近似参数。为便于化简成 Meijer-G 函数, 对 b' 进行向上取整, $b = [b']$, 并利用 $a' + b'x \approx a + bx$ 近似确定 a 。

令 $t = I_m / (I_a I_g)$, 利用文献[34]中 $Q(x) = \exp(-x^2/2)/12 + \exp(-2x^2/3)/4$ 和式(29)可将式(27)表示为

$$P_{\text{SIMO}} = \int_0^\infty \left\{ \frac{1}{12} \exp \left\{ -\frac{1}{2} \left[\sqrt{\frac{2(P_i \hbar I_a I_g G)^2}{\sigma^2}} \frac{t}{M} \right]^2 \right\} + \frac{1}{4} \exp \left\{ -\frac{2}{3} \left[\sqrt{\frac{2(P_i \hbar I_a I_g G)^2}{\sigma^2}} \frac{t}{M} \right]^2 \right\} \right\} \left\{ \frac{b \exp(2a) t^{b-1}}{[1 + \exp(2a) t^b]^2} \right\} dt, \quad (30)$$

根据文献[35]中 Meijer-G 函数的性质 $(1+x)^\phi = \frac{1}{\Gamma(-\phi)} G_{1,1}^{1,1} \left(x \middle|_0^{\phi+1} \right)$ 和 $\exp(-x) = G_{0,1}^{1,0} \left(x \middle|_1^- \right)$ 可将式(30)表示为

$$P_{\text{SIMO}} = b \exp(2a) \int_0^\infty \left\{ \frac{1}{12} G_{0,1}^{1,0} \left[\frac{1}{2} \left[\sqrt{\frac{2(P_i \hbar I_a I_g G)^2}{\sigma^2}} \frac{t}{M} \right]^2 \middle|_1^- \right] + \frac{1}{4} G_{0,1}^{1,0} \left[\frac{2}{3} \left[\sqrt{\frac{2(P_i \hbar I_a I_g G)^2}{\sigma^2}} \frac{t}{M} \right]^2 \middle|_1^- \right] \right\} t^{b-1} \times G_{1,1}^{1,1} \left[\exp(2a) t^b \middle|_1^- \right] dt, \quad (31)$$

式中, $G[\cdot]$ 表示 Meijer-G 函数。

利用文献[35]中式(21)表示的 Meijer-G 函数的积分性质解析式对式(31)进行去积分可推导得到采用 EEGC 的海洋 SIMO 系统 ABER 的闭合解析式:

$P_{\text{SIMO}} \approx$

$$2 \exp(2a) \left(\frac{b}{2\pi} \right)^{\frac{b+1}{2}} \left\{ \frac{1}{12} \left[\frac{\sqrt{2} M}{\sqrt{2(P_t \hbar I_a I_g G)^2 / \sigma^2}} \right]^b G_{2, 2+b}^{2+b, 2} \left\{ \begin{matrix} -1/2, 0, \frac{i-b/2}{b}, b^b \\ 0, 1/2 \end{matrix} \right\} \exp(2a) \left[\frac{\sqrt{2} M}{\sqrt{2(P_t \hbar I_a I_g G)^2 / \sigma^2}} \right]^b \right\}^2 + \frac{1}{4} \left[\frac{\sqrt{1.5} M}{\sqrt{2(P_t \hbar I_a I_g G)^2 / \sigma^2}} \right]^b G_{2, 2+b}^{2+b, 2} \left\{ \begin{matrix} -1/2, 0, \frac{i-b/2}{b}, b^b \\ 0, 1/2 \end{matrix} \right\} \exp(2a) \left[\frac{\sqrt{1.5} M}{\sqrt{2(P_t \hbar I_a I_g G)^2 / \sigma^2}} \right]^b \right\}^2 \quad (32)$$

式中, $i = 1, 2, \dots, b$ 。

5 仿真与数据分析

为分析水体分层的不稳定度、APD分布方式和分集接收合并算法对采用高斯光束传输的弱海洋 SIMO 通信系统性能的影响,进行仿真分析。海洋湍流仿真参数设置为: $\eta = 0.003, \lambda = 532 \text{ nm}, L = 55 \text{ m}, P_{rT} = 7, P_{rs} = 700, P_{rTS} = 13.86, C_T = 2.181, C_s = 2.221, \Theta_0 = 1, C_{TS} = 2.205, \omega_0 = 1 \times 10^{-4}, \chi_T = 1 \times 10^{-7} \text{ K}^2/\text{s}^3, \epsilon = 1 \times 10^{-5} \text{ m}^2/\text{s}^3, L_0 = 10 \text{ m}$ 。在 4 组不同的海洋湍流信道: $d_r = 0.540, \omega = -0.75; d_r = 1.000, \omega = -0.75; d_r = 1.000, \omega = -2.50; d_r = 4.437, \omega = -2.50$ 中,根据式(15)和式(22)可以数值计算得到高斯光束的闪烁指数(SI)和空间相干半径 ρ_0 ,在此基础上可分别确定接收端 APD 间距阈值下限(1 cm)及湍流强度相应的均值和方差。在 SIMO 系统中设置 $M = 3$ 进行模拟计算,得到系统在不同湍流信道中对应的式(29)中非线性拟合系数 a', b' 以及近似参数 a, b ,如表 1 所示。

设 SIMO 系统仿真参数为: $c = 0.151 \text{ m}^{-1}, \Delta l = 4 \text{ cm}, d_A = 0.002 \text{ m}, R_L = 20 \Omega, B = 100 \text{ MHz}, T = 256 \text{ K}, G = 50, \hbar = 0.8 \text{ A/W}$ 。利用式(32)仿真 APD 的放置方式、分集接收合并算法、水体分层的不稳定度对复合弱海洋湍流信道下的 SIMO 系统 ABER 与发射功率的关系,结果如图 3 所示。当 SIMO 通信系统的 ABER 达到 10^{-8} 时,对应的发射功率如表 2 和表 3 所示。对比图 3 和表 2、3 可知,无论采用 EGC 算法或是 EEGC 算法,盐度波动主导 ($\omega = -0.75, d_r = 0.540$)

的弱海洋湍流与水体分层视为稳定状态 ($\omega = -0.75, d_r = 1.000$) 的弱海洋湍流相比, SIMO 通信系统的性能高出约 5.8 dB; 然而温度波动主导 ($\omega = -2.50, d_r = 4.437$) 的弱海洋湍流与水体分层视为稳定状态 ($\omega = -2.50, d_r = 1.000$) 的弱海洋湍流相比, SIMO 通信系统的性能低了约 5.2 dB。这是由对实际海洋湍流中水体分层不稳定性考虑不充分导致的闪烁误差引起的。此外,与温度波动主导 ($\omega = -2.50, d_r = 4.437$) 的弱海洋湍流相比,盐度波动主导 ($\omega = -0.75, d_r = 0.540$) 的海洋湍流中 SIMO 通信系统性能低了约 1.5~1.7 dB。

进一步分析图 3 可知,当 SIMO 通信系统的 ABER 达到 10^{-8} 时,对比表 2 中 APD 位置采用对称分布 ($D_i = 0$) 和表 3 中 APD 位置采用非对称分布 ($D_i = 0.01 \text{ m}$) 的 EGC 算法, APD 对称分布的 EGC SIMO 通信系统性能比 APD 非对称分布通信系统高约 1.5 dB; 当采用 EEGC 算法时,表 2 中 APD 对称分布和表 3 中 APD 非对称分布的 SIMO 通信系统性能相差仅有 0.1 dB。因此,在高斯光束的海洋湍流 SIMO 系统中,采用传统 EGC 算法的系统性能对 APD 的放置位置比较敏感,而所提出的 EEGC 算法的 SIMO 通信系统性能对 APD 放置位置不敏感。此外,从图 3(a)、(b) 及表 2 可知,当接收端 APD 位置为对称分布时,采用 EEGC 算法的 SIMO 通信系统性能比 EGC 算法改进了约 1 dB; 由图 3(c)、(d) 及表 3 可知,当接收端 APD 位置为非对称分布时,采用 EEGC 算法的 SIMO 通信系统性能比 EGC 算法改善了约 2.4 dB。这表明,无论 APD 阵列采用对称还是非对称分布,EEGC 算法均可改善基于高斯光束的 SIMO 通信系统的传输性能。

表 1 55 m SIMO 系统不同海洋湍流信道 PDF 对应的 a, b 值

Table 1 Corresponding coefficients a and b in 55 m SIMO system with respect to different oceanic channels PDFs

d_r	ω	ρ_0/m	SI	Mean and variance of the PDF		Fitting parameter		Approximate parameter	
				Mean	Variance	a'	b'	a	b
-0.540	-0.75	0.0022	0.5569	0.5247	0.0246	-2.7216	5.2037	-3.5784	6
1.000	-0.75	0.0017	0.9546	0.4830	0.0663	-1.5260	3.1877	-2.3037	4
1.000	-2.50	0.0040	0.1336	0.5478	0.0015	-11.5700	21.1246	-12.7643	22
4.437	-2.50	0.0024	0.4515	0.5329	0.0164	-3.3809	6.3585	-4.0947	7

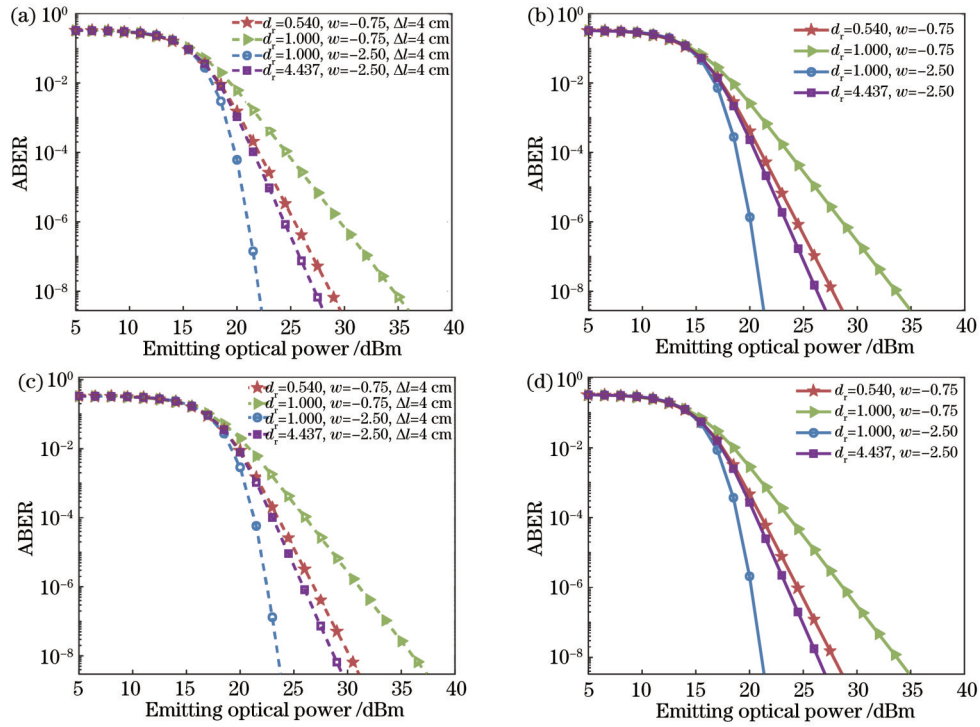


图 3 海洋 SIMO 通信系统 ABER 随发射功率的变化曲线。(a) APD 对称分布的 EGC 算法;(b) APD 对称分布的 EEGC 算法;(c) APD 非对称分布的 EGC 算法;(d) APD 非对称分布的 EEGC 算法

Fig. 3 ABER variation curves of oceanic SIMO communication system with emitting optical power. (a) EGC with symmetrically distributed APD; (b) EEGC with symmetrically distributed APD; (c) EGC with asymmetrically distributed APD; (d) EEGC with asymmetrically distributed APD

表 2 当 APD 对称分布的 SIMO 通信系统 ABER 取 10^{-8} 时所对应的发射光功率

Table 2 Emitting optical power at an ABER of 10^{-8} in SIMO system with symmetrically distributed APD

d_r	ω	Emitting optical power using EGC	Emitting optical power using EEGC
		P_t / dBm	P_t / dBm
0.540	-0.75	28.9	27.7
1.000	-0.75	34.5	33.5
1.000	-2.50	22.0	21.0
4.437	-2.50	27.2	26.2

表 3 当 APD 非对称分布的 SIMO 通信系统 ABER 取 10^{-8} 时所对应的发射光功率

Table 3 Emitting optical power at an ABER of 10^{-8} in SIMO system with asymmetrically distributed APD

d_r	ω	Emitting optical power using EGC	Emitting optical power using EEGC
		P_t / dBm	P_t / dBm
0.540	-0.75	30.1	27.8
1.000	-0.75	36.0	33.6
1.000	-2.50	23.5	21.1
4.437	-2.50	28.7	26.3

采用上述相同的仿真参数,并设置编码参数 $n = 63$ 、 $k_H = 51$,利用式(26)结合式(32)仿真分析采用高

斯光束传输的 RS 编码联合 SIMO 技术的复合通信系统性能,分析不同的分集接收合并算法、水体分层不稳定程度、APD 放置方式对系统上限 ABER 与发射光功率的需求关系,结果如图 4 所示。当系统的上限 ABER 达到 10^{-8} 时,对应的发射光功率如表 4 和表 5 所示。对比图 3 和图 4 可知,相比于未编码的 SIMO 系统,在基于高斯光束传输的 RS 编码联合 SIMO 通信系统中,无论采用 EGC 算法还是 EEGC 算法,RS 编码联合 SIMO 的复合通信系统的性能都得到了较大改善。对比表 2 和表 4 或表 3 和表 5 的数据可知:当系统的 ABER 达到 10^{-8} 时,相比于未编码的 SIMO 通信系统,在盐度波动主导 ($\omega = -0.75$ 、 $d_r = 0.540$) 的弱海洋湍流中,RS 编码联合 SIMO 通信系统性能改善了约 8.1 dB;在盐度波动主导且将水体分层视为稳定状态 ($\omega = -0.75$ 、 $d_r = 1.000$) 的弱海洋湍流中,RS 编码联合 SIMO 通信系统的性能改善了约 12.1 dB;在温度波动主导 ($\omega = -2.50$ 、 $d_r = 4.437$) 的弱海洋湍流中,RS 编码联合 SIMO 通信系统的系统性能改善了约 7 dB;在温度波动主导且将水体分层视为稳定状态 ($\omega = -2.50$ 、 $d_r = 1.000$) 的弱海洋湍流中,RS 编码联合 SIMO 通信系统的性能改善了约 3 dB。对比表 4 和表 5 可知,RS 编码联合 EEGC 算法的 SIMO 系统可大程度地抑制海洋湍流效应对系统性能的影响,并且对 APD 的位置不敏感。此外,观察到在不同的湍流环境

下,RS 编码技术对 SIMO 通信系统性能的改善作用存在很大的差异,这是由不同海洋信道中闪烁指数不同导致的。结合表 1 的数据进一步分析可得,在弱海洋

湍流信道中,湍流强度越大,相比于未编码的通信系统,RS 编码联合 EEGC SIMO 通信系统对湍流的抑制作用越显著。

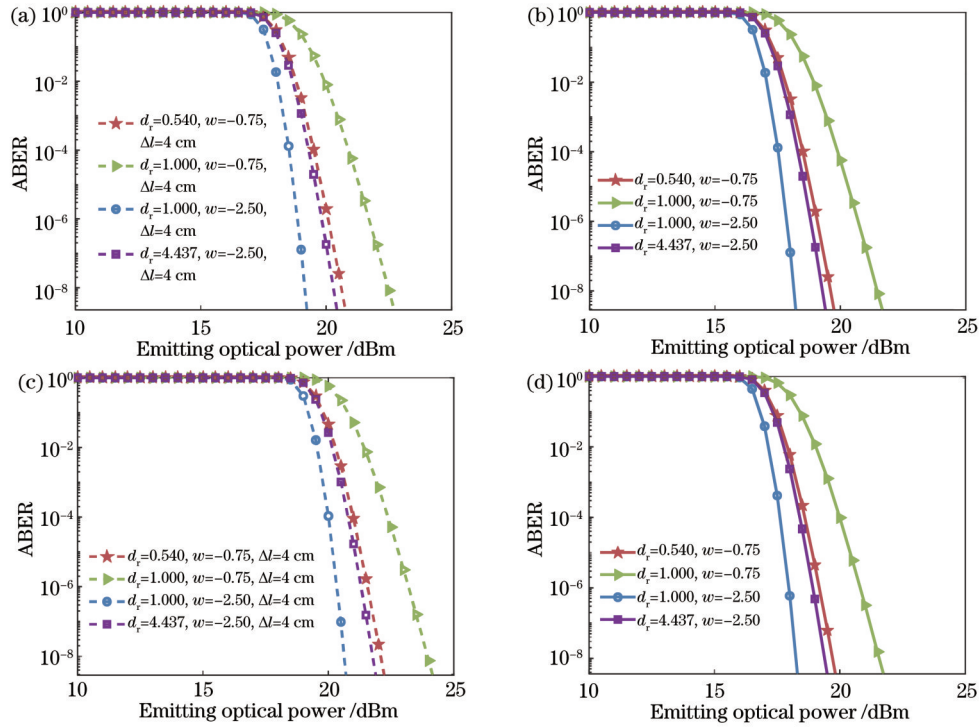


图 4 RS 编码联合 SIMO 通信系统的上限 ABER 随发射功率的变化曲线。(a) APD 对称分布的 EGC 算法;(b) APD 对称分布的 EEGC 算法;(c) APD 非对称分布的 EGC 算法;(d) APD 非对称分布的 EEGC 算法

Fig. 4 Upper bound ABER variation curves of SIMO communication system combined RS codes with emitting optical power. (a) EGC with symmetrically distributed APD; (b) EEGC with symmetrically distributed APD; (c) EGC with asymmetrically distributed APD; (d) EEGC with asymmetrically distributed APD

表 4 APD 对称分布的 RS-SIMO 通信系统上限 ABER 取 10^{-8} 时所对应的发射光功率

Table 4 Emitting optical power at an upper bound ABER of 10^{-8} in RS-SIMO system with symmetrically distributed APD			
d_r	ω	Emitting optical power using EGC P_1 /dBm	Emitting optical power using EEGC P_1 /dBm
0.540	-0.75	20.6	19.6
1.000	-0.75	22.4	21.4
1.000	-2.50	19.1	18.1
4.437	-2.50	20.2	19.2

表 5 当 APD 非对称分布的 RS-SIMO 通信系统上限 ABER 取 10^{-8} 时所对应的发射光功率

Table 5 Emitting optical power at an upper bound ABER of 10^{-8} in RS-SIMO system with asymmetrically distributed APD			
d_r	ω	Emitting optical power using EGC P_1 /dBm	Emitting optical power using EEGC P_1 /dBm
0.540	-0.75	22.0	19.7
1.000	-0.75	23.9	21.5
1.000	-2.50	20.6	18.2
4.437	-2.50	21.7	19.3

6 结 论

基于 Peng Yue 谱推导了高斯光束在海洋水体分层不稳定及外尺度有限的弱海洋湍流中的闪烁指数和空间相干半径闭合解析式,确定了基于高斯光束的 SIMO 通信系统的湍流强度及探测器间距阈值;针对 SIMO 通信系统中接收平面内光强的高斯分布特性提出了一种光强均衡的 EEGC 算法,并建立了基于高斯光束的 RS 编码联合 EEGC SIMO 复合通信系统,利用双曲正切分布法推导了该系统的上限 ABER 的闭合

解析式。仿真分析了不同海洋水体分层不稳定度、APD 分布方式、分集接收算法对 RS 编码联合 SIMO 通信系统性能的影响。研究结果证明,在盐度波动或温度波动主导的光学海洋湍流中,将海洋水体分层视为稳定状态会严重低估或高估海洋 SIMO 通信系统的性能。此外,针对海洋中高斯光束传输特性建立的 RS 编码联合 EEGC SIMO 技术的复合湍流抑制系统可以显著降低湍流对通信系统的影响,并且在弱海洋湍流范围内,湍流强度越大,该系统的湍流抑制效果越显著。同样该系统很大程度上消除了接收端 APD 的分

布方式对系统性能的影响。该研究不仅对高阶复杂光束在真实的海洋信道中的传输特性有指导意义,也可采用复杂光束传输的多种湍流抑制技术构建的复合通信系统的水下应用提供有效的理论基础。

参 考 文 献

- [1] Spagnolo G S, Cozzella L, Leccese F. Underwater optical wireless communications: overview[J]. *Sensors*, 2020, 20(8): 2261.
- [2] 曾凤娇, 杨康建, 晏旭, 等. 水下激光通信系统研究进展[J]. *激光与光电子学进展*, 2021, 58(3): 0300002.
Zeng F J, Yang K J, Yan X, et al. Research progress on underwater laser communication systems[J]. *Laser & Optoelectronics Progress*, 2021, 58(3): 0300002.
- [3] Hill R J. Optical propagation in turbulent water[J]. *Journal of the Optical Society of America*, 1978, 68(8): 1067-1072.
- [4] 季秀阳, 殷洪玺, 景连友, 等. 基于强波动理论的强湍流信道水下无线光通信系统性能分析[J]. *光学学报*, 2022, 42(18): 1801001.
Ji X Y, Yin H X, Jing L Y, et al. Performance analysis of underwater wireless optical communication system with strong turbulence channels based on strong fluctuation theory[J]. *Acta Optica Sinica*, 2022, 42(18): 1801001.
- [5] Nikishov V V, Nikishov V I. Spectrum of turbulent fluctuations of the sea-water refraction index[J]. *International Journal of Fluid Mechanics Research*, 2000, 27(1): 82-98.
- [6] Ata Y, Baykal Y. Scintillations of optical plane and spherical waves in underwater turbulence[J]. *Journal of the Optical Society of America A*, 2014, 31(7): 1552-1556.
- [7] Lu L, Ji X L, Baykal Y. Wave structure function and spatial coherence radius of plane and spherical waves propagating through oceanic turbulence[J]. *Optics Express*, 2014, 22(22): 27112-27122.
- [8] Gerçekcioğlu H. Bit error rate of focused Gaussian beams in weak oceanic turbulence[J]. *Journal of the Optical Society of America A*, 2014, 31(9): 1963-1968.
- [9] Wang Z Q, Zhang P F, Qiao C H, et al. Scintillation index of Gaussian waves in weak turbulent ocean[J]. *Optics Communications*, 2016, 380: 79-86.
- [10] Elamassie M, Uysal M, Baykal Y, et al. Effect of eddy diffusivity ratio on underwater optical scintillation index[J]. *Journal of the Optical Society of America A*, 2017, 34(11): 1969-1973.
- [11] Yue P, Luan X H, Yi X, et al. Beam-wander analysis in turbulent ocean with the effect of the eddy diffusivity ratio and the outer scale[J]. *Journal of the Optical Society of America A*, 2019, 36(4): 556-562.
- [12] Li Y, Zhang Y X, Zhu Y. Oceanic spectrum of unstable stratification turbulence with outer scale and scintillation index of Gaussian-beam wave[J]. *Optics Express*, 2019, 27(5): 7656-7672.
- [13] Luan X H, Yue P, Yi X. Scintillation index of an optical wave propagating through moderate-to-strong oceanic turbulence[J]. *Journal of the Optical Society of America A*, 2019, 36(12): 2048-2059.
- [14] 王建英, 殷洪玺, 季秀阳, 等. 采用 mQAM 和孔径平均的水下弱湍流 MIMO 系统性能分析[J]. *光学学报*, 2021, 41(19): 1901002.
Wang J Y, Yin H X, Ji X Y, et al. Performance analysis of MIMO UWOC systems with weak turbulence channels using mQAM and aperture averaging[J]. *Acta Optica Sinica*, 2021, 41(19): 1901002.
- [15] 赵黎, 王昊, 张峰. 基于光广义空间调制的 VLC-MIMO 系统研究[J]. *中国激光*, 2022, 49(23): 2306001.
Zhao L, Wang H, Zhang F. Research on VLC-MIMO system based on optical generalized spatial modulation[J]. *Chinese Journal of Lasers*, 2022, 49(23): 2306001.
- [16] 文豪, 曹阳, 彭小峰, 等. 自由空间光通信中的 MIMO 极化编码方法[J]. *激光与光电子学进展*, 2021, 58(19): 1906004.
Wen H, Cao Y, Peng X F, et al. MIMO polarization-coding method in free space optical communication[J]. *Laser & Optoelectronics Progress*, 2021, 58(19): 1906004.
- [17] Jiang H Y, He N, Liao X, et al. The BER performance of the LDPC-coded MPPM over turbulence UWOC channels[J]. *Photonics*, 2022, 9(5): 349.
- [18] Du Y T, Li S, Wang P, et al. Performance analysis of multi-hop underwater wireless optical communication system with space-time block codes considering the impact of beam spread function[J]. *Optical Engineering*, 2022, 61(3): 036106.
- [19] Aravind J V, Kumar S, Prince S. Performance analysis of UWOC using SISO and SIMO techniques[J]. *Journal of Physics: Conference Series*, 2021, 1964(6): 062025.
- [20] Liu W H, Xu Z Y, Yang L Q. SIMO detection schemes for underwater optical wireless communication under turbulence[J]. *Photonics Research*, 2015, 3(3): 48-53.
- [21] Boucouvalas A C, Peppas K P, Yiannopoulos K, et al. Underwater optical wireless communications with optical amplification and spatial diversity[J]. *IEEE Photonics Technology Letters*, 2016, 28(22): 2613-2616.
- [22] Jamali M V, Salehi J A, Akhondi F. Performance studies of underwater wireless optical communication systems with spatial diversity: MIMO scheme[J]. *IEEE Transactions on Communications*, 2017, 65(3): 1176-1192.
- [23] Ramavath P N, Udipi S A, Krishnan P. High-speed and reliable underwater wireless optical communication system using multiple-input multiple-output and channel coding techniques for IoT applications[J]. *Optics Communications*, 2020, 461: 125229.
- [24] 吴彤, 季小玲, 李晓庆, 等. 海洋湍流中光波特征参量和短期光束扩展的研究[J]. *物理学报*, 2018, 67(22): 224206.
Wu T, Ji X L, Li X Q, et al. Characteristic parameters of optical wave and short-term beam spreading in oceanic turbulence [J]. *Acta Physica Sinica*, 2018, 67(22): 224206.
- [25] Cox W C. Simulation, modeling, and design of underwater optical communication systems[D]. Raleigh: North Carolina State University, 2012.
- [26] 栾晓晖. 海洋湍流对激光束传播特性的影响研究[D]. 西安: 西安电子科技大学, 2020: 51-52.
Luan X H. Study on the effects of oceanic turbulence on laser beam propagation characteristics[D]. Xi'an: Xidian University, 2020: 51-52.
- [27] Andrews L C, Phillips R L. Laser beam propagation through random media[M]. Bellingham: SPIE, 2005.
- [28] Andrews L C. Special functions of mathematics for engineers [M]. 2nd ed. Bellingham: SPIE, 1998.
- [29] Cheng M J, Guo L X, Zhang Y X. Scintillation and aperture averaging for Gaussian beams through non-Kolmogorov maritime atmospheric turbulence channels[J]. *Optics Express*, 2015, 23(25): 32606-32621.
- [30] Xu F, Khalighi M, Bourennane S. Impact of different noise sources on the performance of PIN- and APD-based FSO receivers[C]//Proceedings of the 11th International Conference on Telecommunications, June 15-17, 2011, Graz, Austria. New York: IEEE Press, 2011: 211-218.
- [31] Cox W C, Simpson J A, Domizioli C P, et al. An underwater optical communication system implementing Reed-Solomon channel coding[C]//OCEANS, September 15-18, 2008, Quebec City, QC, Canada. New York: IEEE Press, 2009.
- [32] Fenton L. The sum of log-normal probability distributions in scatter transmission systems[J]. *IRE Transactions on Communications Systems*, 1960, 8(1): 57-67.

- [33] Kaushal H, Kaddoum G. Underwater optical wireless communication[J]. *IEEE Access*, 2016, 4: 1518-1547.
- [34] Chiani M, Dardari D, Simon M K. New exponential bounds and approximations for the computation of error probability in fading channels[J]. *IEEE Transactions on Wireless Communications*, 2003, 2(4): 840-845.
- [35] Adamchik V S, Marichev O I. The algorithm for calculating integrals of hypergeometric type functions and its realization in REDUCE system[C]//*Proceedings of the international symposium on Symbolic and algebraic computation*, August 20-24, 1990, Tokyo, Japan. New York: ACM Press, 1990: 212-224.

Performance Analysis of the Diversity Receiver System with Reed-Solomon Codes for Oceanic Turbulence Suppression

Yang Yi¹, Qiu Xiaofen^{1*}, Wang Xiaobo², Zhang Jianlei¹, He Hanyu¹, Nie Huan¹, Liu Haoyu¹

¹*School of Electronic Engineering, Xi'an University of Posts & Telecommunications, Xi'an 710121, Shaanxi, China;*

²*Key Laboratory of Underwater Information and Control, China Shipbuilding Industry Corporation 705 Research Institute, Xi'an 710077, Shaanxi, China*

Abstract

Objective With the large-scale deployment of underwater vehicles and ocean sensing networks, underwater high-speed wireless optical communication systems have become an important data acquisition means. The analysis of beam scintillation and transmission characteristics caused by oceanic turbulence and the exploration of effective oceanic turbulence suppression techniques have become a key technology for building underwater wireless laser communication systems with high stability, high speed rate, and long-range transmission. However, the inconsistency of salt transfer and thermal diffusion mechanisms in the real oceanic environment leads to unstable water stratification, and meanwhile, the refractive index power spectrum based on the infinite outer scale results in possible singularity problems at the poles. As a result, the scintillation effects of Gaussian beams in the oceanic turbulence channel and the theoretical model of spatial coherence radius deviate significantly from the real oceanic environment. Therefore, a Gaussian beam-based Reed-Solomon (RS) coded joint single-input multiple-output (SIMO) communication system using the equalized equal gain combining (EEGC) algorithm is developed to further mitigate the light intensity flicker caused by oceanic turbulence and improve the transmission performance of the system under a weak oceanic channel with a finite outer scale and oceanic water stratification instability.

Methods We derive closed analytical formulas for the scintillation index and spatial coherence radius for a Gaussian beam based on Yue spectrum, and quantify the turbulence intensity and the detector spacing threshold in a Gaussian beam-based oceanic diversity receiver system under a weak oceanic turbulence channel with a finite outer scale and oceanic water stratification instability. A Gaussian beam-based composite communication system is proposed. This system combines the RS codes technique with the SIMO technique through the EEGC algorithm in light of the aforementioned study. In addition, a closed analytic formula for the upper bound average bit error rate (ABER) of our proposed system using the hyperbolic tangent distribution method is derived.

Results and Discussions To verify the designed scheme, we employ the derived closed analytical formulas of scintillation index and spatial coherence radius to determine the turbulence intensity and the detector spacing thresholds for four different channels in our proposed composite communication system (Table 1). Based on this, the performance of the Gaussian beam-based RS coded joint SIMO communication system is investigated in detail by numerical simulations under different detector distribution methods and the instability of oceanic water stratification (Fig. 4). When avalanche photodiodes (APDs) in the receiving plane are placed in symmetrical distribution and asymmetric distribution, the emitting optical power at an upper bound ABER of 10^{-8} is summarized in Table 4 and Table 5, respectively. Results show that the performance of our proposed RS coded joint SIMO communication system can be significantly underestimated or overestimated by treating oceanic water stratification as a stable state in optical oceanic turbulence caused by salinity fluctuations or temperature fluctuations (Fig. 4). By further comparing the EEGC SIMO communication system (Fig. 3) with the RS coded joint EEGC SIMO communication system (Fig. 4), the proposed RS coded joint EEGC SIMO communication system can significantly improve the transmission performance of the system under different turbulent channels. Additionally, the improvement in system performance is noticed to be more significant as the oceanic turbulence

intensity increases in the weak oceanic composite channel. Therefore, comparing emitting optical power at an upper bound ABER of 10^{-8} in an RS-SIMO system with symmetrically and asymmetrically distributed APDs, it can be seen that the performance of the RS coded joint SIMO system with symmetric distributed APDs is about 1.5 dB better than that of the asymmetrically distributed APDs RS coded joint SIMO system when the EGC algorithm is adopted. When the APD position at the receiver is symmetrically distributed, the performance of the EEGC algorithm improves by about 1 dB over the EGC algorithm (Table 4). When the APD at the receiver is asymmetrically distributed, the performance of the RS coded joint SIMO system with the EEGC algorithm improves by about 2.4 dB (Table 5). The RS coded joint SIMO communication system using the proposed EEGC algorithm can effectively compensate the system performance loss caused by the non-linearity of the Gaussian beams and reduce the influence of the detector distribution method on the system performance.

Conclusions An EEGC algorithm for light intensity equalization is proposed for the Gaussian distribution characteristics of the light intensity in the receiving plane in the SIMO communication system, and an RS coded joint EEGC SIMO composite communication system based on Gaussian beams is established. The closed analytic formula for the upper bound ABER of the proposed system using the hyperbolic tangent distribution method is further derived. The simulation results show that the instability of the oceanic water stratification exerts a significant influence on the system performance. The designed communication system significantly mitigates the effect of oceanic turbulence on the system's performance, especially the suppression effect, which becomes more significant as the oceanic turbulence intensity increases. Additionally, the proposed system eliminates the influence of the detector distribution on the Gaussian beam-based SIMO system performance. We not only provide guidance for the characteristics of high-order complex beams in real marine channels but also a useful theoretical basis for the underwater applications of composite communication systems using multiple turbulence suppression techniques for complex beam transmission.

Key words wireless optical transmission; oceanic turbulence; Gaussian beam; diversity reception; Reed-Solomon code